On the Distribution of Horizontal Transports by Transient Eddies in the Northern Hemisphere Wintertime Circulation[1]

NGAR-CHEUNG LAU[2] AND JOHN M. WALLACE

Department of Atmospheric Sciences, University of Washington, Seattle, WA 98195

(Manuscript received 13 February 1979, in final form 18 May 1979)

ABSTRACT

Horizontal fluxes of geopotential, heat, zonal momentum, relative vorticity and potential vorticity by the transient eddies on selected pressure surfaces are computed on the basis of data from twice daily synoptic charts for the Northern Hemisphere, objectively analyzed at the National Meteorological Center. The distribution of fluxes is resolved into nondivergent and irrotational parts and displayed in a vectorial format.

The nondivergent flux of geopotential closely parallels contours of constant temporal variance of geopotential. Nondivergent transient eddy fluxes of heat, relative vorticity and potential vorticity, all evaluated in the vicinity of the tropopause level, bear a similar but less exact relation to the distribution of the temporal variance of geopotential. These relationships are shown to exist because 1) the wind field responsible for the fluxes is quasi-geostrophic and 2) the instantaneous distributions of temperature, relative vorticity and potential vorticity tend to be rather similar to that of the geopotential field in the vicinity of the tropopause level. For these three parameters and for geopotential, the nondivergent fluxes at the tropopause level tend to be considerably larger than the corresponding irrotational fluxes.

The distribution of transient eddy heat flux in the lower troposphere is primarily irrotational and directed down the local horizontal gradient of the time-averaged temperature field. The magnitudes of these fluxes are comparable to those of corresponding fluxes associated with horizontal temperature advection by the time-averaged flow. There does not appear to be any simple functional relationship between the scalar magnitudes of the fluxes and local mean temperature gradients. The irrotational transient eddy heat fluxes at 300 mb resemble the distribution of total transient eddy heat flux at 850 mb. At the 200 mb level these fluxes are primarily countergradient in middle latitudes.

The irrotational transient eddy flux of zonal momentum at the jet stream level is much smaller than the corresponding flux associated with momentum advection by the time-averaged flow and it is directed into regions of low zonal wind speed. The irrotational flux of geopotential is directed out of regions of decaying transient disturbances and into regions of cyclogenesis.

The irrotational fluxes of vorticity and potential vorticity near the jet stream level are very similar. Their distribution appears to be strongly related to the time-averaged sea level pressure field, with fluxes out of regions of high sea level pressure and into regions of low pressure. These transports appear to be in the proper sense to fulfill the balance requirements for vorticity and potential vorticity. The divergence of the transient eddy flux of potential vorticity is weaker than the horizontal advection of potential vorticity by the time-averaged flow. It is suggested that the observed distribution of potential vorticity flux is imposed on the transient eddies by the distribution of sources and sinks of potential vorticity at the earth's surface which are closely related to the sea level pressure distribution.

1. Introduction

One of the primary objectives of general circulation research over the past 30 years has been the documentation, interpretation and understanding of the transient eddy fluxes, so that they can be parameterized in long-range forecasting and climate models. The vast majority of the published works on this topic deal with the rather specialized problem of estimating the zonally averaged eddy fluxes. Although it is much less evident in the refereed literature, a great deal of effort has also been devoted to documenting the distribution of these fluxes as a function of longitude, as well as latitude, height and season. Notable examples include the works

[1] Contribution No. 496, Department of Atmospheric Sciences, University of Washington.

[2] Present affiliation: Geophysical Fluid Dynamics Program, Princeton University, Princeton, NJ 08540.

0022-4928/79/101844-18$08.50

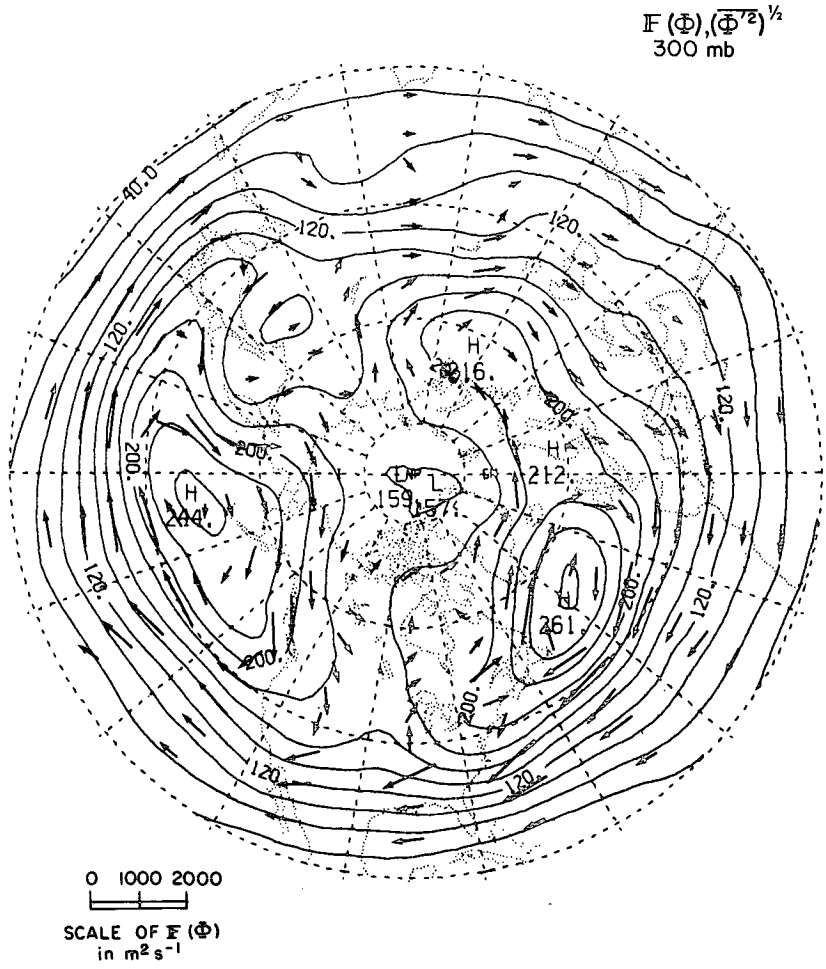

FIG. 1. Vectors show transient eddy flux of geopotential height at the 300 mb level in units of m^2 s^{-1}. The length scale for the vectors is given in the lower left-hand corner of the figure. For conversion to eddy flux of geopotential energy, multiply this scale by 9.81 m s^{-2}. In all figures of this paper, the shafts of the arrows are centered on the grid point in question, arrows too short to show up clearly have been omitted. Contours show the square root of the temporal variance of 300 mb height; contour interval, 20 m. In this and other figures displayed on polar stereographic projections, the meridians and latitude circles are drawn at an interval of 20°, the outermost latitude circle represents 20°N.

of Buch (1954),[3] Peixoto (1960)[4] and Obasi (1963),[5] which were carried out within the Massachusetts Institute of Technology Planetary Circulations Project, under the direction of Victor P. Starr, and the studies of Newell *et al.* (1972, 1974). More recently, A. H. Oort has compiled an extensive set of hemispheric analyses of transient eddy flux statistics based on a special collection of 15 years of upper air sounding data; plans are underway to publish these charts in the form of microfilm.

Progress in documenting the three-dimensional distributions of the horizontal fluxes by transient eddies has been hampered by the spatial inhomogeneity of the radiosonde network. In the absence of theoretical relationships to serve as constraints on the analysis, it has been difficult to justify the interpolation of the patterns of transient eddy fluxes over the large, data-sparse regions of the globe.

[3] Buch, H., 1954: Hemispheric wind conditions during the year 1950. Final Report, Part 2, U.S. Air Force Contract No. AF19-122-153, Planetary Circulations Project, Dept. of Meteorology, MIT, Cambridge, MA 02139.

[4] Peixoto, J. P., 1960: Hemispheric temperature conditions during the year 1950. Sci. Rep. No. 4, U.S. Air Force Contract No. AF19(604)-6108, Planetary Circulations Project, Dept. of Meteorology, MIT, Cambridge, MA 02139.

[5] Obasi, G. O. P., 1963: Atmospheric momentum and energy calculations for the Southern Hemisphere during the IGY. Sci. Rep. No. 6, U.S. Air Force Contract No. AF19(604)-6108, Planetary Circulations Project, Dept. of Meteorology, MIT, Cambridge, MA 02139.

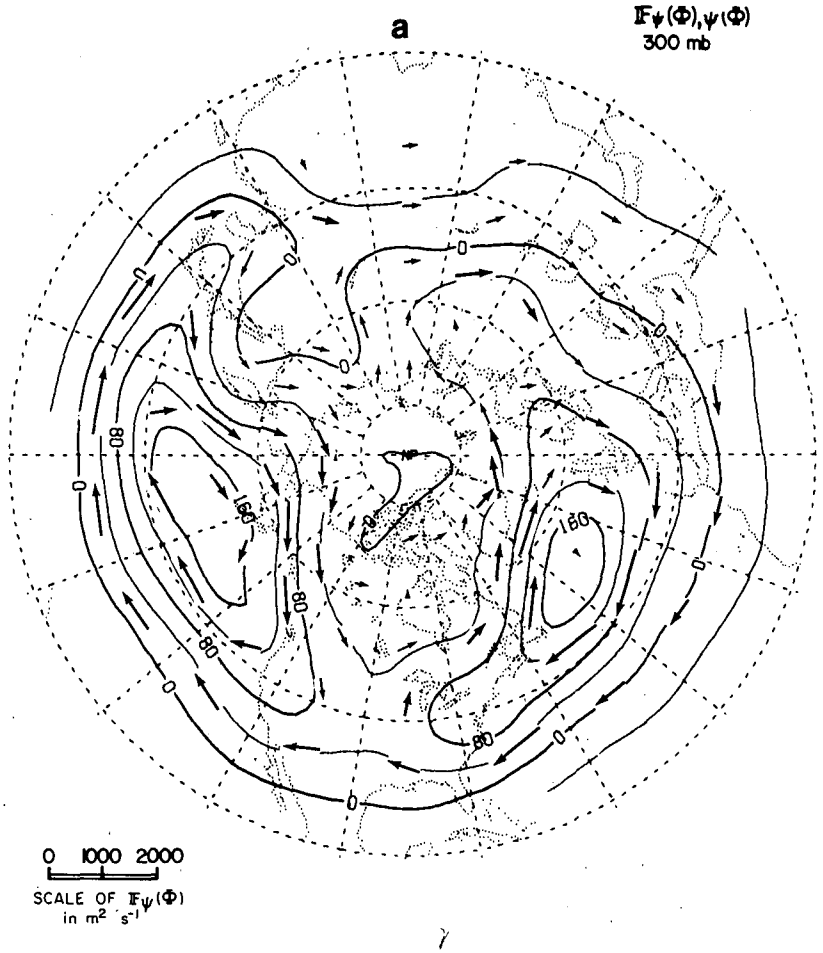

FIG. 2. (a) Vectors show nondivergent transient eddy flux of geopotential height at the 300 mb level (units of m^2 s^{-1}). The length scale for the vectors is given in the lower left hand corner of the figure. For conversion to eddy flux of geopotential energy, multiply this scale by 9.81 m s^{-2}. Contours show the corresponding streamfunction; contour interval 4×10^8 m^3 s^{-1}. (b) As in (a), but for irrotational flux (vectors) superimposed on its velocity potential (contours); contour interval 4×10^7 m^3 s^{-1}.

Another stumbling block has been the seemingly overwhelming amount of information inherent in the three-dimensional distributions of the transient eddy fluxes. In the absence of some sort of "organizing principle," it is difficult to assimilate all this information and effectively incorporate it into climate models.

In the present paper, we hope to demonstrate that these problems can be overcome, to a large extent, by deriving the transient eddy flux statistics from gridded hemispheric synoptic analyses rather than from station data, and by expanding the resulting vector fields of the horizontal transient eddy fluxes in terms of nondivergent and irrotational parts. The rationale for this procedure is as follows: The hemispheric synoptic analyses contain a considerable amount of information from sources other than radiosondes (e.g., reports from merchant ships and commercial aircraft, bogusing of cloud patterns revealed by satellite imagery, time continuity from the previous analysis). Furthermore, such analyses routinely make use of the hypsometric equation and the gradient wind relation as constraints which are helpful in interpolating the wind and temperature fields onto a regularly spaced grid in data-sparse regions. Our analysis procedure also takes advantage of the fact that the "flux streamfunctions" and "flux potential functions" respectively associated with the nondivergent and irrotational parts of the transient eddy fluxes display patterns which are spatially more coherent than the corresponding patterns in the meridional or zonal components of the fluxes themselves. The broad features of the flux streamfunctions and flux potential functions are more easily identified and analyzed, particularly in data sparse regions. By

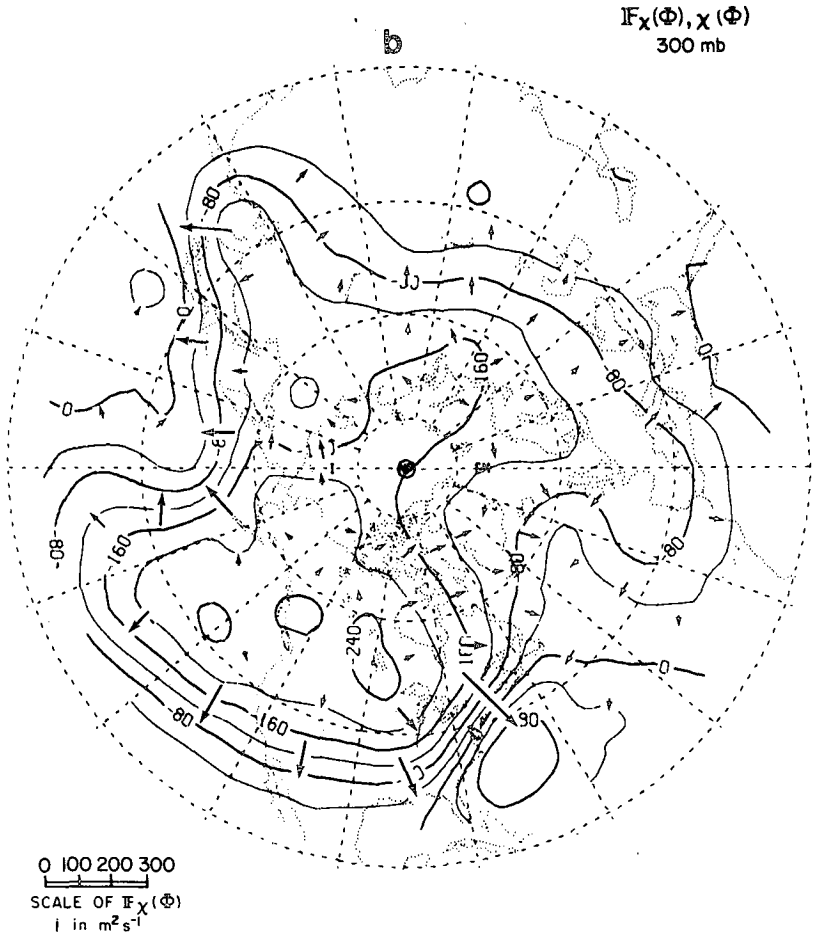

FIG. 2. (*Continued*)

means of examples, we will attempt to show that the expansion in terms of nondivergent and irrotational components provides the needed "organizing principle" that makes it possible to describe (qualitatively, at least) the horizontal fluxes of geopotential, heat, vorticity and potential vorticity throughout a wide range of vertical levels in the atmosphere in terms of a small number of relatively simple patterns. For the purpose of studying the forcing of the time-averaged flow by the transient eddies the irrotational fluxes are of primary interest. The observed relationships between the irrotational fluxes and the time-averaged wind and temperature fields offer some possible clues as to how the transient eddies might be parameterized in time-averaged climate models.

For the sake of conciseness and clarity, we will display the horizontal transient eddy fluxes in a vectorial format. For this purpose, we define the time-averaged horizontal flux of the scalar quantity x by transient eddies as

$$\mathbb{F}(x) \equiv \overline{u'x'}\mathbf{i} + \overline{v'x'}\mathbf{j} = \overline{\mathbb{V}'x'}, \qquad (1)$$

where overbars denote time averages, primes denote deviations from time averages,[6] and $\mathbf{i}$ and $\mathbf{j}$ are the unit vectors in the zonal and meridional directions, defined in accordance with the usual meteorological usage, so that $\overline{u'x'}$ and $\overline{v'x'}$ are the zonal and meridional fluxes of x by transient eddies, and $\mathbb{V}$ is the horizontal wind vector. A similar vectorial mapping scheme was used by Peixoto (1960, Plate 184)[4] for displaying the vertically integrated heat transport, and by Starr *et al.* (1965, Fig. 2) for displaying the horizontal eddy flux of water vapor. Some of the vector flux fields are further decomposed into nondivergent and irrotational parts:

[6] In the current series of papers, the transient eddy statistics are first computed for each individual winter, and these statistics are then averaged over the 11 winter seasons from 1965/66 to 1975/76, i.e., the primes appearing in $\overline{u'x'}$ and $\overline{v'x'}$ represent deviations of the data values within a certain winter from the seasonal average for that particular winter. The transient eddy transports presented in this paper were computed using the unfiltered time series of twice daily analyses produced by the U.S. National Meteorological Center. The winter season is taken to be the 120-day period starting from 15 November.

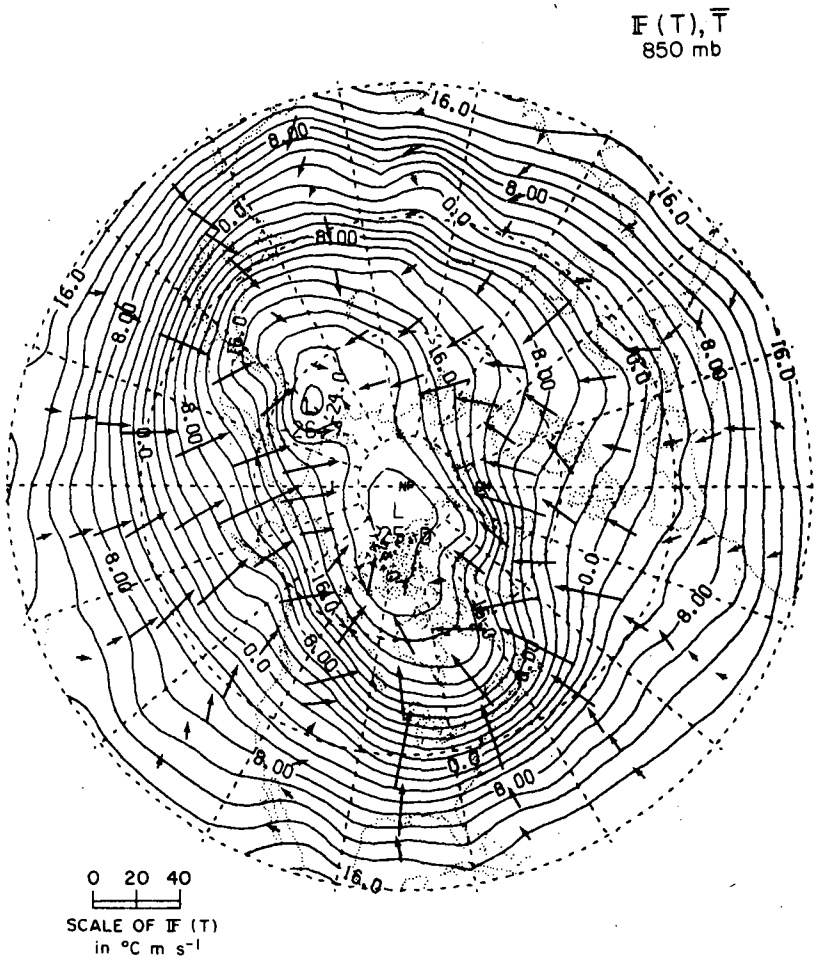

FIG. 3. Vectors show transient eddy heat flux at the 850 mb level, in units of °C m s^{-1}. Contours show mean 850 mb temperature; contour interval, 2°C.

$$\mathbf{F}(x)^{\sim} = \mathbf{F}_{\psi}(x) + \mathbf{F}_{\chi}(x), \tag{2}$$

where

$$\mathbf{F}_{\psi}(x) = \mathbf{k} \times \nabla\psi(x) \tag{3a}$$

and

$$\mathbf{F}_{\chi}(x) = \nabla\chi(x) \tag{3b},$$

Here ∇ is the horizontal gradient operator, and $\mathbf{k}$ is the vertical unit vector. The flux streamfunction ψ and the flux potential function χ are obtained by determining the distributions of the curl and horizontal divergence of the field of $\mathbf{F}(x)$, respectively, and solving the Poisson's equations[7]

$$\nabla^2\psi(x) = \mathbf{k}\cdot\nabla \times \mathbf{F}(x) \tag{4a}$$

and

$$\nabla^2\chi(x) = \nabla\cdot\mathbf{F}(x). \tag{4b}$$

A similar formulation in terms of nondivergent and irrotational fluxes has been used by Rosen *et al.* (1979) for investigating the horizontal eddy transport of water vapor.

To forestall future confusion, it is extremely important to note at the outset that the expansion in terms of nondivergent and irrotational parts is used in an unconventional way in this paper, in the sense that we are applying it to the fluxes, and not to the wind field responsible for the fluxes. In many cases the nondivergent component of the horizontal wind field makes the dominant contribution not only to $\mathbf{F}_{\psi}(x)$, but to $\mathbf{F}_{\chi}(x)$ as well. The above formulation should also not be confused with the resolution of $\mathbf{F}(x)$ into components directed parallel and perpendicular to the horizontal gradient of $\bar{x}$, as was done by Clapp (1970) and Tucker (1977), although such a resolution could easily be applied

[7] The NCAR software subroutine PWSSSP (NCAR, 1978) was used to invert the Laplacian in spherical coordinates. Unless otherwise indicated, the boundary conditions that $\psi = 0$ and $\chi = 0$ at 20°N latitude have been used. The solutions for regions poleward of 30°N were found to be not very sensitive to the choice of boundary conditions at 20°N. For a more detailed discussion of the solutions to these Poisson type equations, see Shukla and Saha (1974).

to the distributions shown in Figs. 3 and 6 of our paper.

In certain cases we shall compare the irrotational transient eddy fluxes with the horizontal fluxes associated with advection of the corresponding quantity by the time-averaged motion field. For this purpose we make use of the relation

$$\nabla^2\Omega(x) = \nabla\cdot\bar{\mathbf{V}}\bar{x} = \bar{\mathbf{V}}\cdot\nabla\bar{x} + \bar{x}\nabla\cdot\bar{\mathbf{V}}, \qquad (5)$$

where $\Omega(x)$ is the potential function for the flux of x by the mean flow. Since the Laplacian operator is linear, we can write

$$\Omega(x) = \Omega_{\mathrm{ADV}}(x) + \Omega_{\mathrm{DIV}}(x), \qquad (6)$$

where

$$\nabla^2\Omega_{\mathrm{ADV}}(x) = \bar{\mathbf{V}}\cdot\nabla\bar{x},$$

$$\nabla^2\Omega_{\mathrm{DIV}}(x) = \bar{x}\nabla\cdot\bar{\mathbf{V}}.$$

Here $\Omega_{\mathrm{ADV}}(x)$ is the contribution of the horizontal advection term in (5) to $\Omega(x)$, and $\Omega_{\mathrm{DIV}}(x)$ is the contribution of the horizontal divergence term. The

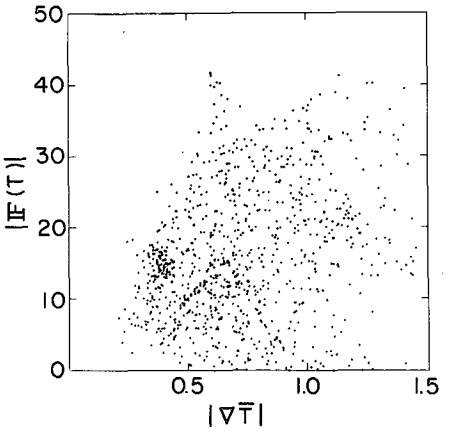

FIG. 4. Scatter diagram for the magnitude of the downgradient component of the transient eddy heat flux versus the magnitude of the local, time-averaged horizontal temperature gradient, based on data in Fig. 3. The units for the y axis (heat fluxes) and x axis (temperature gradients) are expressed in °C m s^{-1} and 10^{-5} °C m^{-1}, respectively. Each point in the scattergram represents the 11 winter average values at an individual grid point. All grid points between 30° and 60°N are included in the figure.

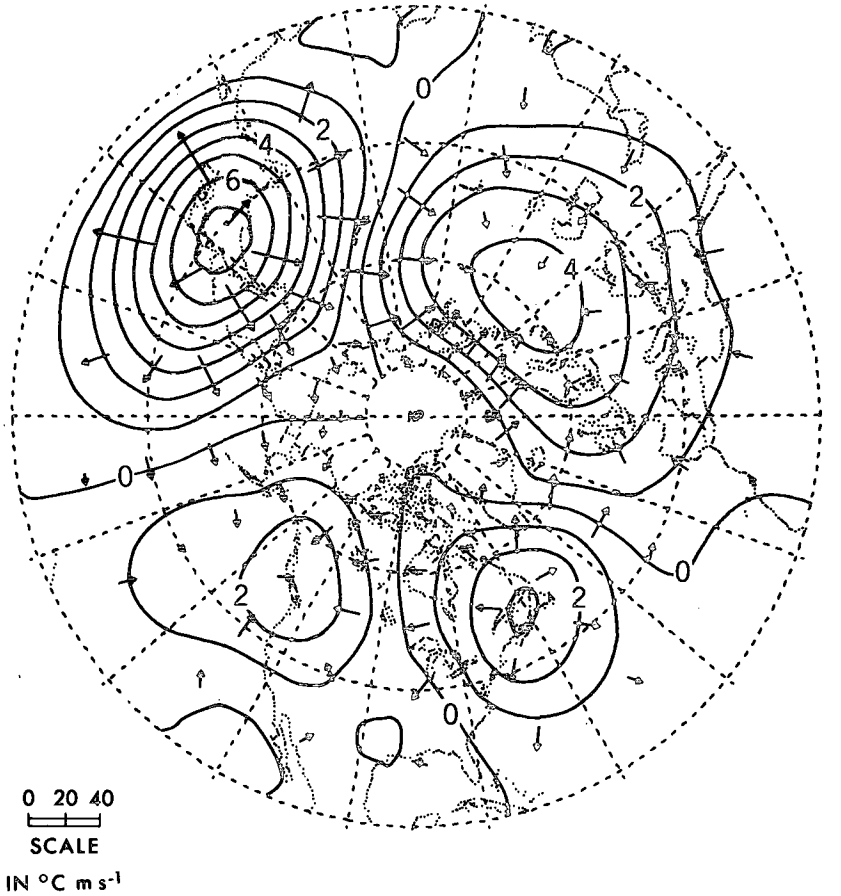

FIG. 5. Vectors show the gradient field of $\Omega_{\mathrm{ADV}}(T)$ at 850 mb, as defined in Eq. (6). Contours show the distribution of $\Omega_{\mathrm{ADV}}(T)$ at the same level; contour interval 1×10^7 °C m^2 s^{-1}.

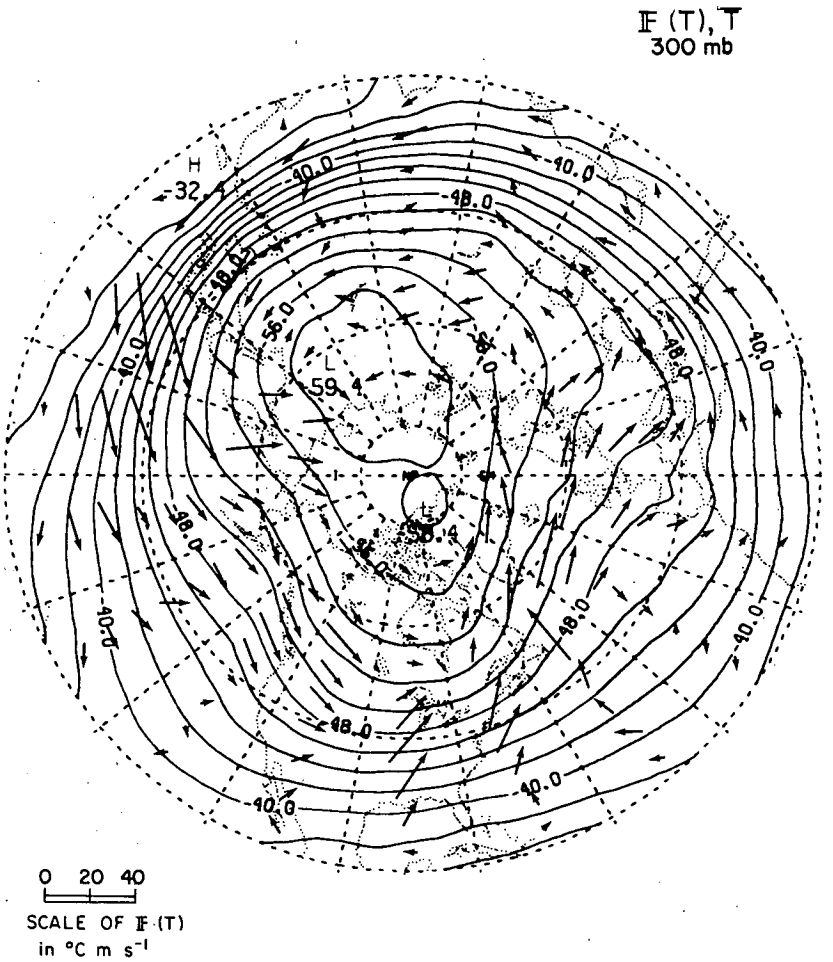

FIG. 6. Vectors show the transient eddy heat flux at 300 mb. Contours show 300 mb mean temperature; contour interval, 2°C.

horizontal gradient of $\Omega_{ADV}(x)$ is an irrotational vector field which can be compared with $\mathbf{F}_\chi(x)$ in order to contrast the roles of advection by the mean flow and transient eddy fluxes in the horizontal transport of x.

2. Geopotential energy fluxes

In Fig. 1 is shown the horizontal transport of geopotential energy $\mathbf{F}(\Phi)$ at 300 mb, as depicted by the arrows. The contours of the root-mean-square (rms) field of geopotential Φ (expressed in terms of geopotential height) at the same level are superimposed on the same figure. As was pointed out by Lau (1978), the strong correspondence between the two fields should not be surprising in view of the relationship

$$\mathbf{F}(\Phi) \approx \overline{\mathbf{V}_g'\Phi'} = \frac{1}{2f}\mathbf{k} \times \nabla\overline{\Phi'^2} \qquad (7)$$

which is obtained directly from the geostrophic wind equation. Here $\mathbf{V}_g$ is the geostrophic component of the wind vector, and f is the Coriolis parameter. A physical interpretation of this relationship for the special case of an elongated maximum in the $\overline{\Phi'^2}$ field (or "storm track") has been given in Lau *et al.* (1978, Figs. 6 and 7).

Since a substantial part of $\mathbf{F}(\Phi)$ is nondivergent, the geographical distribution of the divergence features of this field cannot be discerned readily from inspection of Fig. 1. A resolution of the $\mathbf{F}(\Phi)$ field into nondivergent and irrotational fluxes, as defined by (2), is shown in Fig. 2.[8] The nondivergent flux, shown superimposed on its streamfunction $\psi(\Phi)$ in Fig. 2a is virtually indistinguishable from the total $\mathbf{F}(\Phi)$ field in Fig. 1. The irrotational flux, shown superimposed upon its potential field $\chi(\Phi)$ in Fig. 2b is much weaker, but it shows a consistent pattern with a divergence of geopotential flux away from

[8] The boundary condition that $\partial\psi(\Phi)/\partial y = -\overline{u'\Phi'}$ at 20°N latitude has been used to solve Poisson's equation $\nabla^2\psi(\Phi) = \mathbf{k}\cdot\nabla \times \mathbf{F}(\Phi)$.

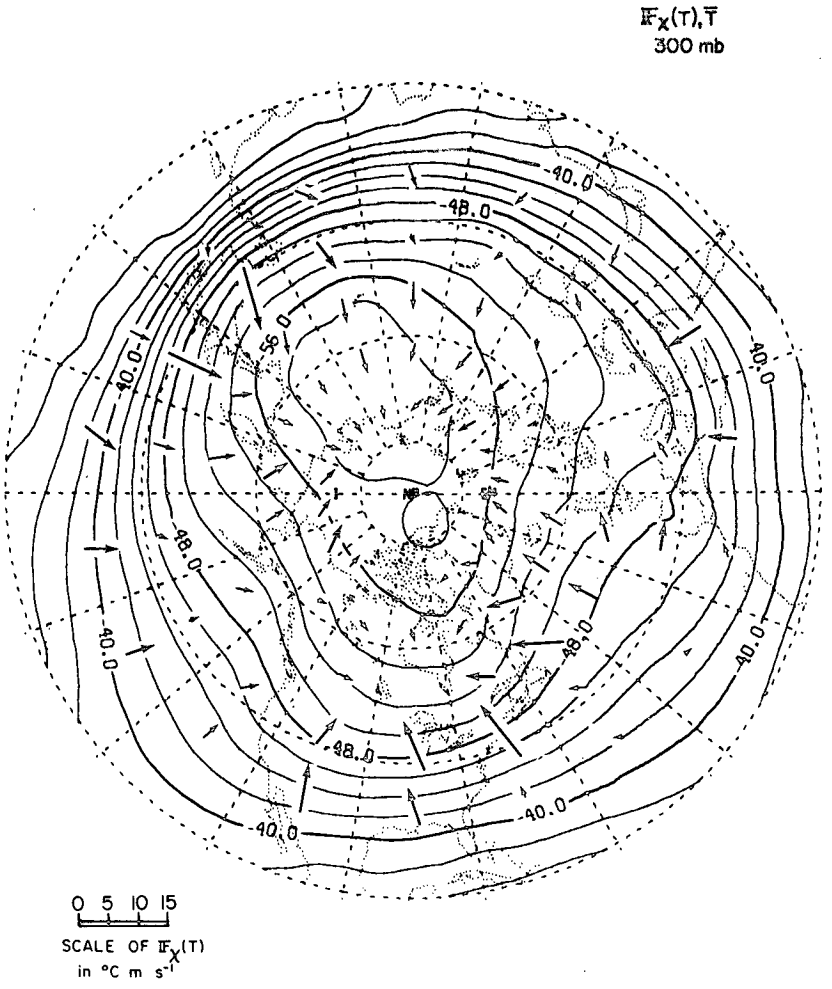

FIG. 7. Vectors show the irrotational transient eddy heat flux at 300 mb. Contours show 300 mb mean temperature; contour interval, 2°C.

the west coasts of Europe and North America, and convergence into the regions adjacent to the east coasts of the continents. The former regions are preferred sites for decaying disturbances, and the latter regions are preferred sites for the genesis of baroclinic waves (see, e.g., Lau 1979a).

Comparison of the local values of $\nabla\cdot\overline{\mathbf{V}_g'\Phi'}$ and $\nabla\cdot\overline{\mathbf{V}'\Phi'}$ (not shown) indicates that the latter are relatively stronger by a factor of more than 3; hence the divergence of $\overline{\mathbf{V}_g'\Phi'}$ due to the latitudinal variation of the Coriolis parameter makes only a minor contribution to the patterns shown in Fig. 2b in comparison to the effects of organized ageostrophic motions. The contribution of these ageostrophic fluxes to the local generation of kinetic energy in the transient eddies may be examined by making use of the following relationship:

$$f(\overline{u'v_a'} - \overline{v'u_a'}) = -\overline{\mathbf{V}'\cdot\nabla\Phi'} = -\nabla\cdot\overline{\mathbf{V}'\Phi'} + \overline{\Phi'(\nabla\cdot\mathbf{V})'}, \quad (8)$$

where the subscripts a refer to ageostrophic components. The distribution of the generation of transient eddy kinetic energy $f(\overline{u'v_a'} - \overline{v'u_a'})$ at 300 mb has already been shown in Lau (1979a, Fig. 11) in connection with the eddy kinetic energy budget. That distribution bears a strong similarity to the divergence pattern of the vector fluxes depicted in Fig. 2b. The values of the principal maxima and minima in the distributions of $f(\overline{u'v_a'} - \overline{v'u_a'})$ and $\nabla\cdot\overline{\mathbf{V}'\Phi'}$ (not shown) are well within a factor of 2 of one another. Hence, the patterns in Fig. 2b can be interpreted in terms of the prevalence of cross-isobar flow toward higher pressure over the western continents and cross-isobar flow toward lower pressure over the western oceans.

3. Heat fluxes

a. The 850 mb level

In Fig. 3 is shown the pattern of transient eddy heat fluxes $\mathbb{F}(T)$ at the 850 mb level, superimposed

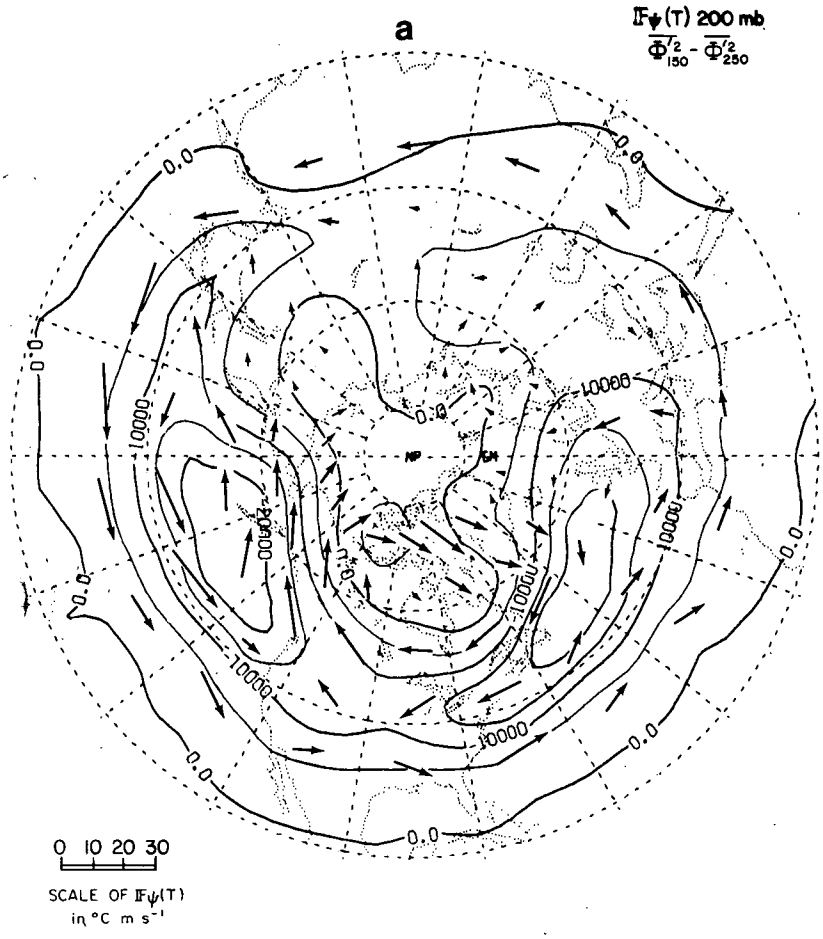

FIG. 8. Vectors show (a) nondivergent and (b) irrotational transient eddy heat flux; both at the 200 mb level. Contours represent (a) temporal variance of 150 mb geopotential height minus temporal variance of 250 mb geopotential height; contour interval, 5000 m^2; and (b) 200 mb mean temperature; contour interval, 2°C.

on the time-averaged temperature field at the same level. It is evident that this field is primarily irrotational, i.e., $\mathbf{F}(T) \simeq \mathbf{F}_\chi(T)$ at 850 mb. The fluxes show a strong tendency to be directed down the local temperature gradient from higher toward lower temperatures. This property is also evident in the patterns for individual winters (not shown). Hence the transient eddies are not only acting to reduce the zonally averaged meridional temperature gradient, but also the east-west temperature gradients associated with the standing wave pattern. The divergence field of the transient eddy heat flux at 700 mb, which is similar to that at 850 mb, has been shown explicitly and discussed in Lau (1979b, Fig. 20c) in the context of the local heat balance. In view of the apparent relationship between the local temperature gradient vector and the direction of the heat fluxes in Fig. 3, it is of interest to examine whether any functional relationship exists between the magnitudes of the heat fluxes and local temperature gradients. Fig. 4 shows a scatter diagram for the magnitude of the downgradient component of $\mathbf{F}(T)$ at 850 mb versus the magnitude of the local, time-averaged horizontal temperature gradient. There is little evidence of any consistent relationship between the magnitudes of the heat fluxes and local temperature gradients. Nor have we been able to identify consistent relationships between fluxes and gradients for the eleven individual winters at any given grid point.

It is interesting to compare the magnitude and spatial distribution of the transient eddy heat fluxes $\mathbf{F}(T)$ at the 850 mb level with the transports required to account for the horizontal advection by the time-averaged flow at the same level. The latter transports, as derived from (5) and (6), are displayed in Fig. 5. It can be seen that the transient eddy heat fluxes and the fluxes associated with horizontal temperature advection by the mean flow are roughly comparable in terms of magnitude but much different in terms of spatial distribution. The mean flow produces a divergence of heat out of the regions of

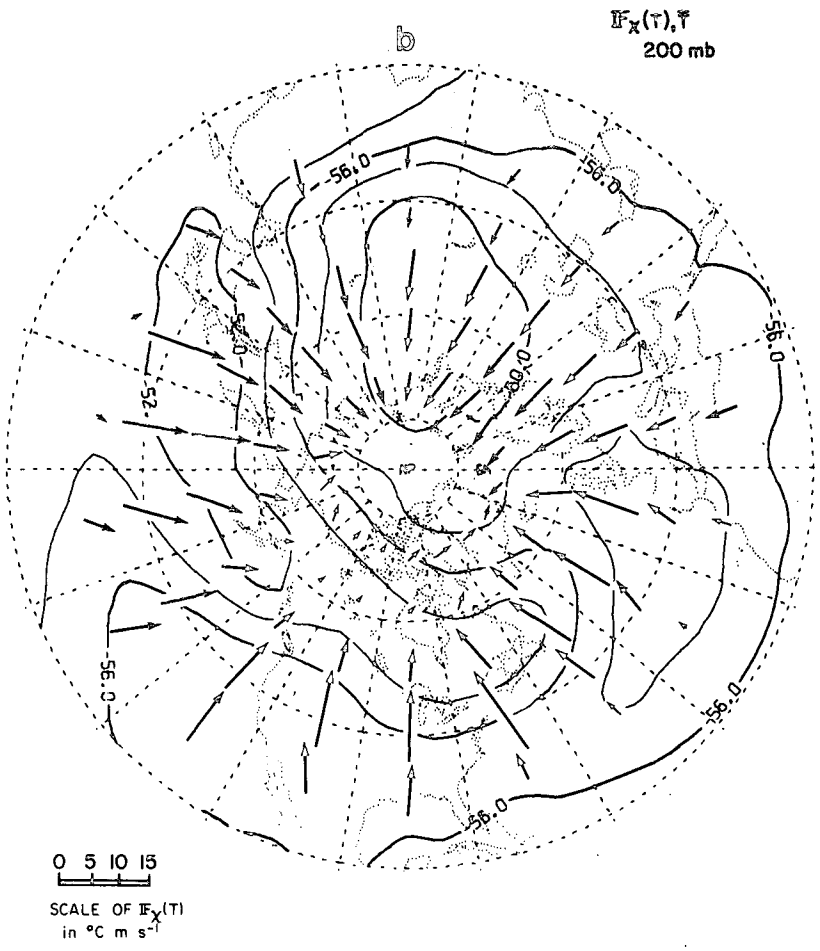

FIG. 8 (*Continued*)

cold advection over Japan and eastern Canada and a convergence of heat into the regions of warm advection centered over northwestern North America and the European part of the Soviet Union. It is evident that in the zonal average, the mean flow produces a net poleward flux of heat.

b. The 300 mb level

The distributions of the transient eddy heat flux and time averaged temperature at 300 mb are shown in Fig. 6. The fluxes tend to be aligned with local mean temperature contours over the eastern oceans and the adjacent land areas. It is evident from this pattern that the meridional component of $\mathbb{F}(T)$ at this level is directed equatorward in the longitudinal sectors corresponding to western North America and western Europe, as was noted in Lau (1978, Figs. 9e and 9f). In Fig. 7 is shown the irrotational transient eddy heat flux $\mathbb{F}_\chi(T)$ at the 300 mb level, superimposed upon the corresponding time mean temperature field. There is a strong resemblance between this pattern and the distribution of total transient eddy heat flux at the 850 mb level (Fig. 3), with the fluxes being mostly directed down the gradient of mean temperature. The magnitudes of $\mathbb{F}_\chi(T)$ at the 300 mb level are about 40% as strong as those at the 850 mb level.

c. The 200 mb level

The nondivergent and irrotational transient eddy heat fluxes at the 200 mb level are shown in Fig. 8. The nondivergent fluxes tend to be larger than the irrotational fluxes by about a factor of two. (The same is true at the 300 mb level.) The vertical structure of transient disturbances in the vicinity of the tropopause level tends to be equivalent barotropic, so that $T' \approx \pm\Phi'/\lambda_z$, where λ_z is proportional to some characteristic vertical scale of the eddies and the sign is positive below the mean tropopause level (e.g., 300 mb) and negative above the mean tropopause level (e.g., 200 mb). Substituting this approximate relationship into (7), we obtain

$$\mathbb{F}(T) \approx \overline{\mathbb{V}_g' T'} \approx \pm \frac{1}{2f\lambda_z} \mathbb{k} \times \nabla\overline{\Phi'^2}. \qquad (9)$$

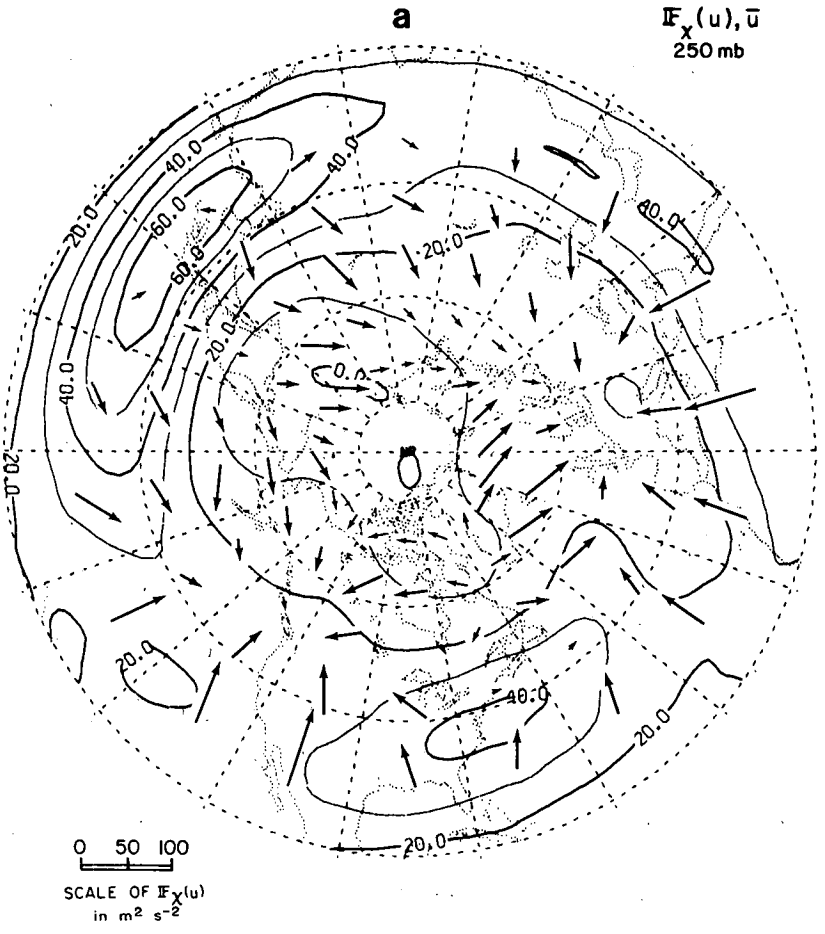

FIG. 9. Vectors show (a) the irrotational transient eddy flux of westerly momentum at 250 mb, and (b) the gradient field of $\Omega_{ADV}(u)$ at the same level, as defined in Eq. (6). Contours in both (a) and (b) show time-averaged zonal wind at 250 mb; contour interval, 10 m s^{-1}.

Hence the transient eddy heat flux vectors $\mathbf{F}(T)$ should tend to parallel the corresponding geopotential flux vectors at the 300 mb level and they should tend to be in the opposite direction at the 200 mb level. These relationships should be particularly apparent in the distribution of the nondivergent flux $\mathbf{F}_\psi(T)$.

The transient eddy heat flux distribution at 300 mb (Fig. 6) is dominated by the nondivergent part and there is indeed a distinct tendency for anticyclonic circulations of the fluxes around the regions of strong eddy activity over the northern oceans (as manifested in the $\overline{\Phi'^2}$ distribution in Fig. 1). This tendency is even more apparent in the nondivergent flux $\mathbf{F}_\psi(T)$ at the 300 mb level (not shown). The expected circulation in the opposite sense is apparent in $\mathbf{F}_\psi(T)$ at the 200 mb level, shown in Fig. 8a. A somewhat more exact "thermal wind" type relationship can be derived by differentiating (7) with respect to pressure and making use of the fact that for equivalent barotropic disturbances, Φ is a separable function of the horizontal coordinates (x,y) and pressure (p), which yields the expression

$$\mathbf{F}(T) \approx \overline{\mathbf{V}_g' T'} \approx \frac{p}{4Rf}\,\mathbf{k} \times \nabla\left(-\frac{\partial}{\partial p}\,\overline{\Phi'^2}\right), \quad (10)$$

where p is pressure and R is the gas constant. The contours in Fig. 8a represent the scalar field of $-\partial/\partial p(\overline{\Phi'^2})$ at the 200 mb level, as obtained by a finite difference approximation, using data for $\overline{\Phi'^2}$ at the 250 and 150 mb levels. The correspondence between the flux vectors and the scalar field is quite good except within the region at high latitudes, where $\overline{\Phi'^2}$ is increasing with height in association with vertically propagating planetary waves; since (10) applies only to equivalent barotropic disturbances, one should not expect to see agreement in that region.

Fig. 8b shows the irrotational transient eddy heat flux, superimposed upon the mean temperature field at the 200 mb level. In contrast to the situation at

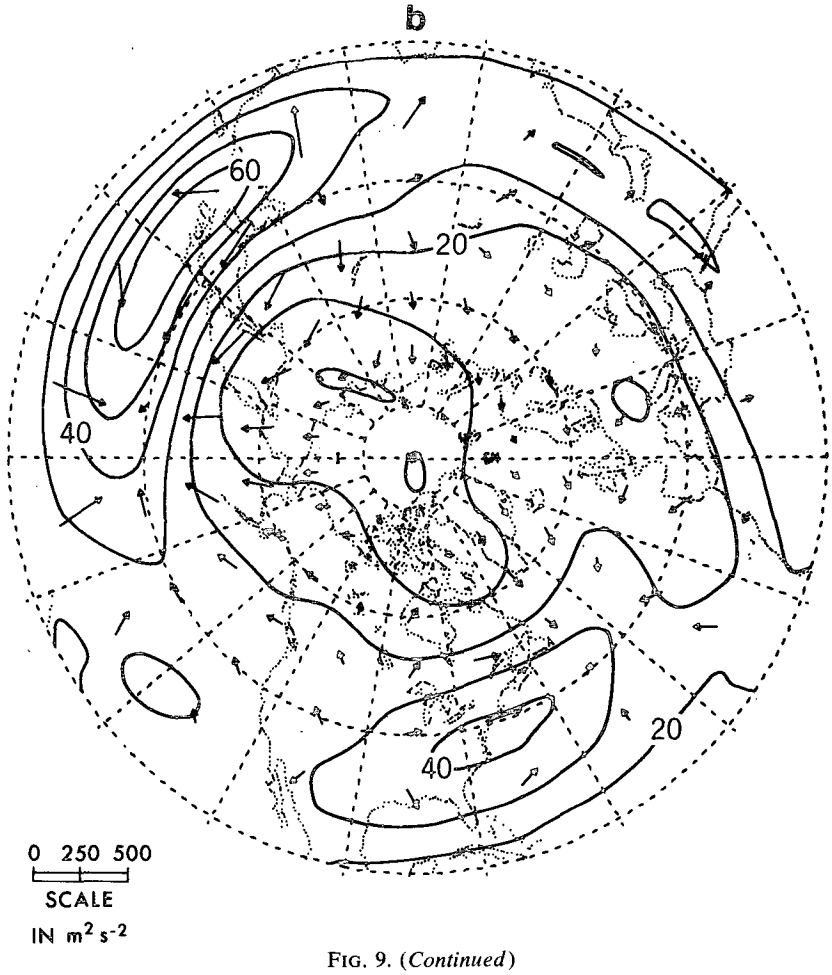

FIG. 9. (*Continued*)

the 850 and 300 mb levels, there is no prevailing tendency for the heat fluxes to be directed from warm regions toward colder regions. The fluxes are predominantly poleward at all longitudes even though the temperature field exhibits strong departures from zonal symmetry. The warm belt stretching from the Gulf of Alaska eastward to Labrador coincides with a region of strong convergence of transient eddy heat flux. The heating rates associated with this convergence are on the order of 1°C day^{-1}, which is comparable to the radiative cooling rates in this region of the atmosphere (e.g., see Dopplick, 1974); but they are a factor of 3 smaller than the corresponding flux divergences associated with the time mean flow field which exhibit an entirely different pattern (not shown) and the adiabatic temperature changes associated with the time mean vertical velocity field. For this reason we are reluctant at this point to make any inferences concerning the forcing of the time mean temperature field by the transient eddy heat fluxes at lower stratospheric levels despite the rather suggestive relationship in Fig. 8b.

4. Momentum fluxes

The irrotational flux of westerly momentum by transient eddies $\mathbf{F}_x(u)$ at the 250 mb level is displayed in Fig. 9a, superimposed on contours of the time-averaged zonal wind component for the same level. The pattern is marked by a strong convergence of $\mathbf{F}_x(u)$ over the western continents, where the zonal flow is relatively weak. There is weak divergence of the flux over the entrance region of the Asian jetstream.

The corresponding fluxes associated with horizontal advection by the time mean flow, as derived from (5) and (6), are shown in Fig. 9b using a reduced scale for determining the length of the arrows. As previously stated by Lau (1978) the fluxes and associated convergences and divergences due to the time mean flow are a factor of 3–5 larger than those associated with the transient eddies; their distribution is characterized by a flux of zonal momentum out of the entrance regions of the major jetstreams, where the advective term $-\bar{u}\partial\bar{u}/\partial x$ is negative, and into the exit regions, where $-\bar{u}\partial\bar{u}/\partial x$ is positive.

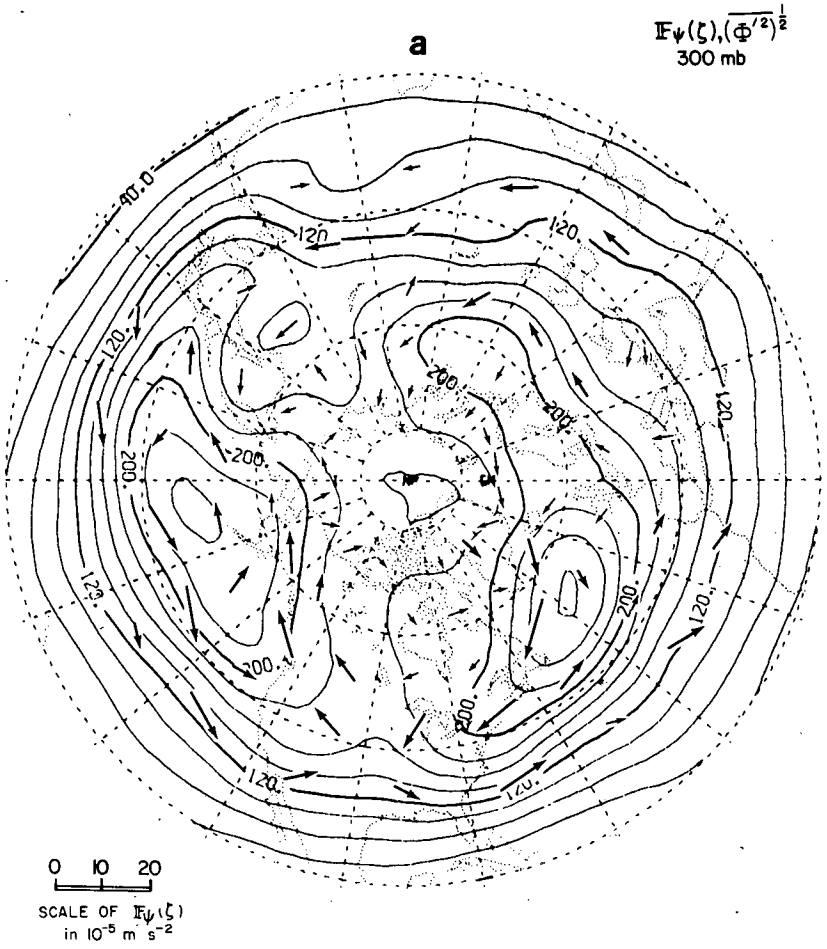

FIG. 10. Vectors show (a) nondivergent and (b) irrotational transient eddy flux of vorticity at 300 mb. Arrows too short to show up clearly have been omitted. Contours show (a) square root of the temporal variance of 300 mb height; contour interval, 20 m; and (b) time-averaged sea level pressure field, expressed in terms of height of the 1000 mb surface; contour interval, 20 m.

5. Vorticity fluxes

Since the horizontal momentum transports by transient eddies ($\overline{u'u'},\overline{u'v'},\overline{v'v'}$) may be related to eddy vorticity fluxes (e.g., Holopainen, 1978), the forcing of the seasonally averaged flow due to these momentum transports may be studied by examining the distribution of vorticity fluxes, and the role of these fluxes in the local, time averaged vorticity balance.

In Fig. 10 are shown the (a) nondivergent and (b) irrotational components of the transient eddy fluxes of relative vorticity ζ at the 300 mb level. (There is no distinction between the transient eddy flux of relative vorticity and absolute vorticity.) The nondivergent flux, which is larger by a factor of about 2, tends to circulate around the contours of $\overline{\Phi'^2}$ (shown superimposed in the figure) in the opposite sense as the flux of geopotential. This relationship follows directly from (7) if we assume that the transient eddies are quasi-isotropic in the horizontal so that $\zeta' \approx -\Phi'/\lambda_H^2$, where λ_H is proportional to some characteristic horizontal length scale of the transient eddies.

Even though it is the smaller of the two in absolute magnitude, the irrotational flux should be of greater importance from the point of view of the forcing of the time averaged flow. Its distribution appears to be related to the time averaged sea level pressure field (shown superimposed in Fig. 10b) with $\mathbf{F}_\chi(\zeta)$ tending to diverge out of regions of high sea level pressure, and converge into regions of low sea level pressure. The former regions are sources of cyclonic vorticity as far as the atmosphere is concerned, since the frictional drag on the anticyclonic circulations at the earth's surface may be viewed as exerting a cyclonic torque on the atmosphere. In a

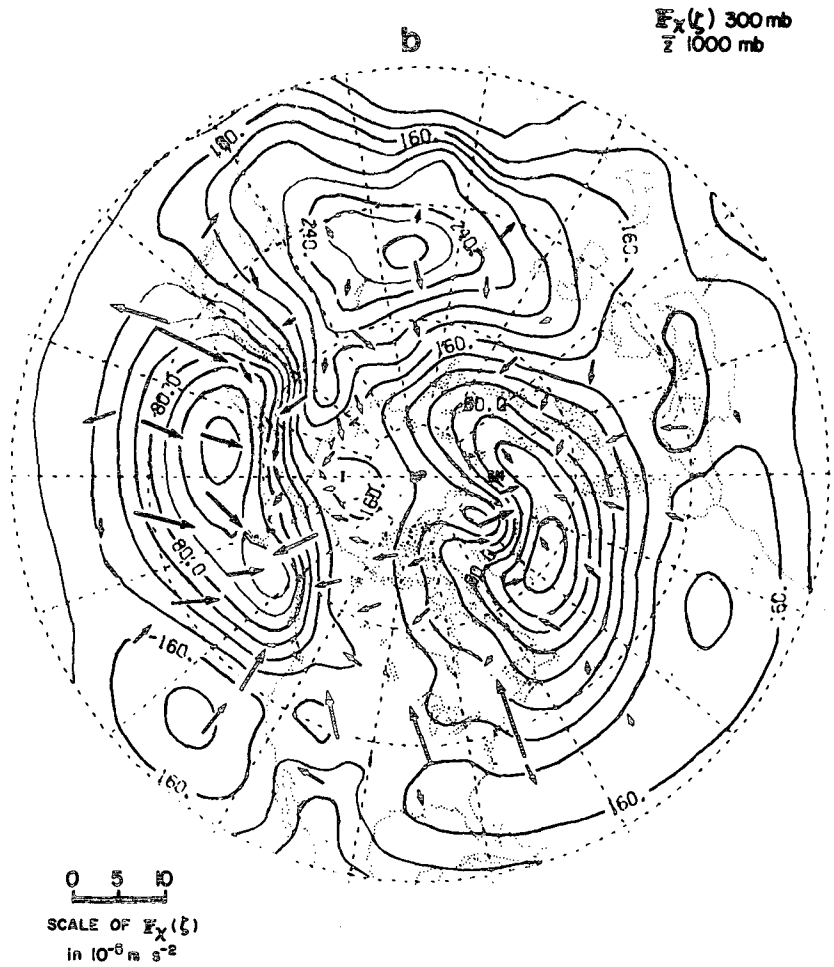

FIG. 10. (*Continued*)

similar manner, the Icelandic and Aleutian surface lows may be viewed as sinks of relative vorticity due to the "spindown" of the cyclonic circulations that surround them.

These fluxes of relative vorticity from source to sink regions are in qualitative agreement with results of a recent study by Holopainen (1978), who also noted that horizontal fluxes by transient eddies play an important role in the vertically averaged budget of vorticity, time-averaged over the annual cycle. However, recent results by Lau (1979b) indicate that for the wintertime averaged circulation, the advection of absolute vorticity by the time averaged flow at the jet stream level is larger than $\nabla\cdot\bar{F}(\zeta)$ by a factor of about 2. Similar conclusions were reported by Benton (1954)[9] and Clapp (1956), based on the analysis of shorter data sets.

[9] Benton, G. S., 1954: Atmospheric studies of large-scale transfer fields over the North American Continent, Part IV. [Final Rep. V. 1, Contract AF19(122)-365], Johns Hopkins University, 248 pp.

6. Potential vorticity fluxes

The transports of potential vorticity are related to heat and momentum fluxes, and provide for a measure of the net forcing of the time mean flow due to transient motions (e.g., Saltzman, 1962). It is therefore of interest to understand how the transient eddies transport potential vorticity in the atmosphere, and the manner in which such transports fulfill the balance requirements for potential vorticity.

The Ertel potential vorticity at the 200 mb level is approximated in this study by the quantity

$$P \equiv -(\zeta + f)\frac{\partial\theta}{\partial p}, \qquad (11)$$

where the relative vorticity ζ is evaluated on constant pressure surfaces and the vertical derivative of potential temperature $\partial\theta/\partial p$ is estimated locally by taking the difference between the values of θ evaluated at the 250 and 150 mb levels. Hartmann (1977) has shown that these are adequate approxi-

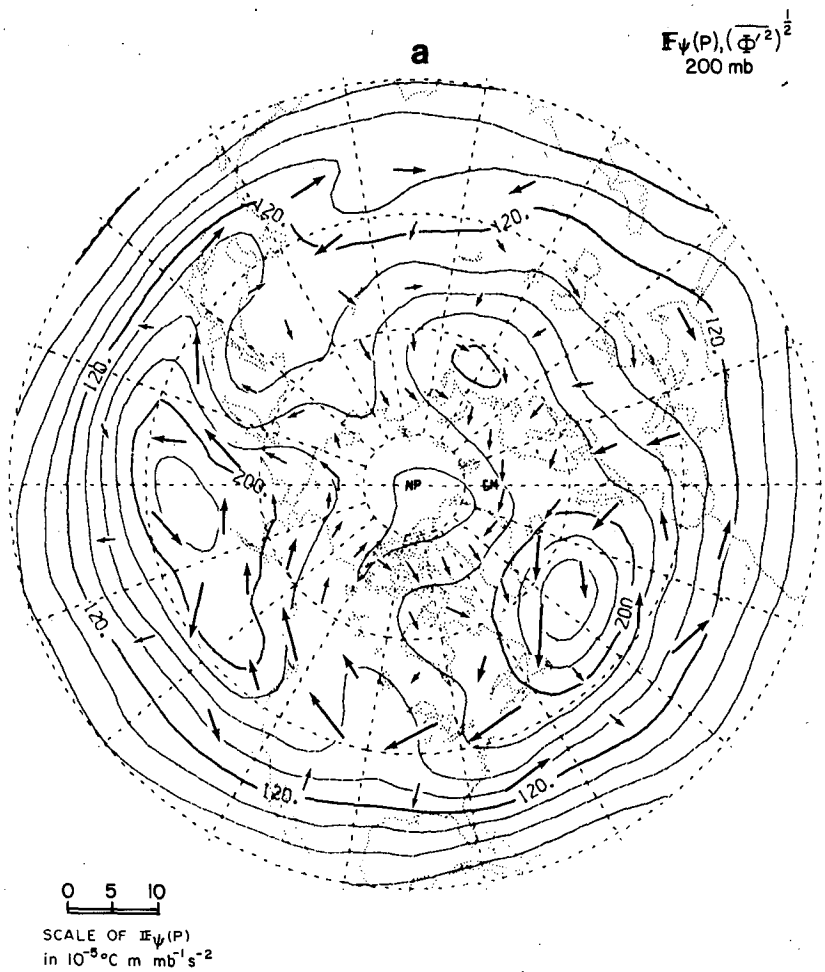

FIG. 11. Vectors show (a) nondivergent and (b) irrotational transient eddy flux of Ertel potential vorticity at 200 mb, as defined in Eq. (11). Arrows too short to show up clearly have been omitted. Contours show (a) square root of the temporal variance of 200 mb height; contour interval, 20 m and (b) time-averaged height of the 1000 mb surface; contour interval, 20 m.

mations for large-scale flows in a hydrostatic and highly stratified atmosphere, with $Ro \ll 1$ and $RiRo^2 \geq 1$, where Ro, Ri are the Rossby and Richardson numbers, respectively. The distributions of the nondivergent and irrotational fluxes of potential vorticity are shown in Fig. 11.

The nondivergent flux $\mathbf{F}_\psi(P)$, whose distribution is shown in Fig. 11a is rather noisy, but it tends to circulate cyclonically around centers of strong transient eddy activity (as defined by the temporal variance of the 200 mb height field), in a manner analogous to $\mathbf{F}_\psi(\zeta)$. Since relative vorticity and static stability exhibit a strong positive correlation in the vicinity of the jetstream level, it is reasonable that the transient eddy fluxes of relative vorticity and potential vorticity should have similar distributions. This similarity is even more apparent in the distribution of the irrotational flux $\mathbf{F}_\chi(P)$ shown in Fig. 11b, which is characterized by a divergence of potential vorticity out of the time mean surface anticyclones and a convergence into the semipermanent surface cyclones over the northern oceans. It seems likely that these regions correspond, respectively to sources and sinks of potential vorticity at the earth's surface. In the surface anticyclones over the continents not only is cyclonic vorticity being generated as a result of the cyclonic frictional torque on the atmosphere, but also the static stability is being increased as a result of cooling from below. Meanwhile, over the northern oceans, cyclonic circulations are spinning down and static stability is being destroyed by the strong input of heat from the ocean surface and from latent heat release in the lower troposphere. Hence it appears that the transient eddies transport potential vorticity from source to sink regions.

It is interesting to compare the distribution of $\mathbf{F}_\chi(P)$ with the horizontal fluxes associated with

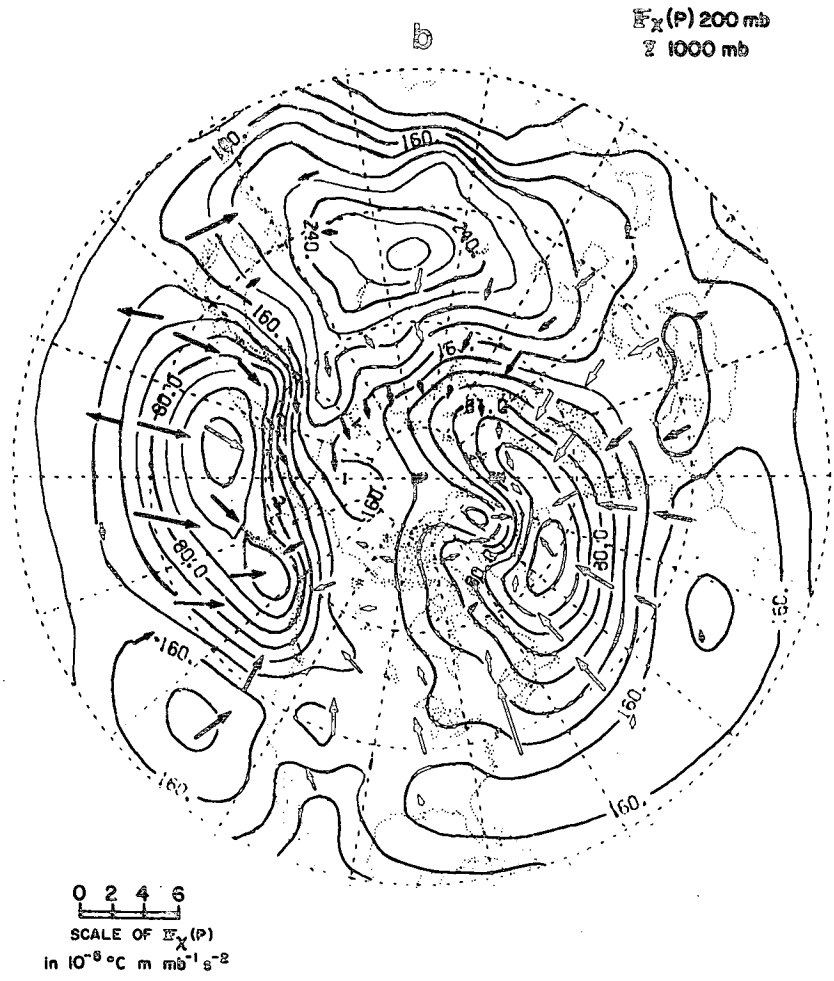

FIG. 11. (*Continued*)

advection by the time mean flow, as derived from (5) and (6), which are shown in Fig. 12. The two distributions are remarkably similar in terms of their shape, but the fluxes associated with potential vorticity advection by the mean flow are larger, by a factor of 2 or 3, and appear to be even more strongly related to the sea level pressure pattern.

7. Interpretation

The observational results described in the previous sections strongly suggest that the nature of the horizontal transient eddy fluxes of geopotential, heat, vorticity and potential vorticity can be described in terms of a few simple patterns which are related to basic structural characteristics of the transient eddies as follows:

1) The nondivergent fluxes of all four parameters have streamfunctions which resemble the distribution of the temporal variance of geopotential height $\overline{\Phi'^2}$.

2) The observed dominance of $\mathbf{F}_\psi(\Phi)$ (relative to $\mathbf{F}_\chi(\Phi)$) and the strong resemblance of its streamfunction to the distribution of $\overline{\Phi'^2}$ is a direct consequence of the quasi-geostrophy of the horizontal wind field, as demonstrated in Eq. (7).

3) The observed dominance of $\mathbf{F}_\psi(T)$ (relative to $\mathbf{F}_\chi(T)$) above the 500 mb level and the resemblance of its streamfunction to the distribution of $\overline{\Phi'^2}$ is indicative of an approximate proportionality between T' and Φ', which results from the nearly equivalent barotropic vertical structure of the transient eddies in the upper troposphere and lower stratosphere.

4) The observed dominance of $\mathbf{F}_\psi(\zeta)$ (relative to $\mathbf{F}_\chi(\zeta)$) near the jet stream level, and the resemblance of its streamfunction to the distribution of $\overline{\Phi'^2}$ is indicative of an approximate proportionality between ζ' and Φ', which results from a nearly isotropic horizontal structure of the transient eddies.

5) The observed dominance of $\mathbf{F}_\psi(P)$ [relative to $\mathbf{F}_\chi(P)$] near the jet stream level, and the resemblance of its streamfunction to the distribution of $\overline{\Phi'^2}$ in the vicinity of the tropopause level is indicative of an approximate proportionality between P' and Φ',

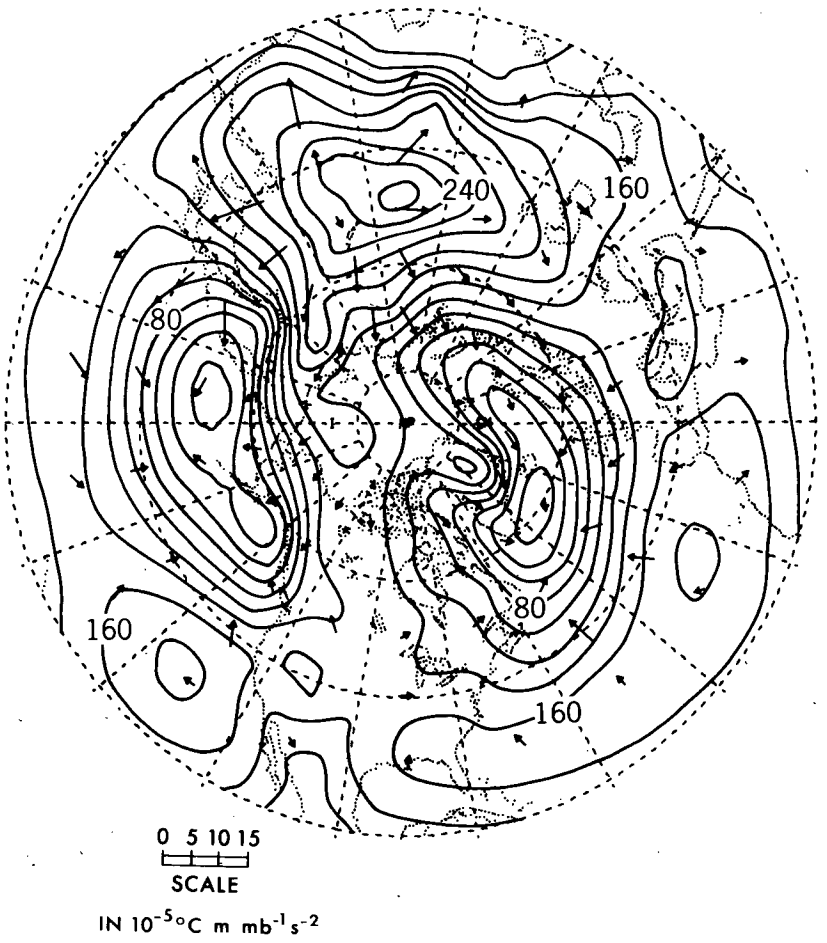

FIG. 12. Vectors show the gradient field of $\Omega_{ADV}(P)$ at 200 mb, as defined in Eq. (6). Contours show time-averaged geopotential height of the 1000 mb surface; contour interval, 20 m.

which serves as further evidence that the wind field in the transient eddies is nearly equivalent barotropic and horizontally isotropic.

6) The wind field in the transient eddies could be completely equivalent barotropic and horizontally isotropic only if the eddies were horizontally homogeneous (i.e., if the $\overline{\Phi'^2}$ field had no horizontal gradients), in which case, there could be no horizontal transient eddy fluxes of Φ, T, ζ and P by the geostrophic wind field [see Eqs. (7) and (10)]. Hence the nondivergent fluxes referred to above are apparently a consequence of the weak baroclinicity and horizontal anisotropy that exist by virtue of the uneven stirring of the upper troposphere and lower stratosphere, which gives rise to horizontal gradients of transient eddy amplitude. Although these nondivergent fluxes do not force the mean flow, it is important to be aware of their existence in interpreting the transient eddy flux statistics in localized regions (e.g., Tucker 1977).

7) The irrotational flux of geopotential appears to be closely related to the distribution of cross-isobar flow in the transient eddies. The observed distribution shows a divergence of geopotential flux out of regions of kinetic energy destruction, where $-\overline{\mathbf{V}'\cdot\nabla\Phi'} < 0$ and a convergence into regions of kinetic energy generation, where $-\overline{\mathbf{V}'\cdot\nabla\Phi'} > 0$.

8) The irrotational transient eddy fluxes of T, ζ and P owe their existence to baroclinicity and anisotropy which are related to factors other than the presence of horizontal gradients of eddy amplitude. Irrotational heat fluxes result from baroclinicity associated with systematic vertical tilts of the transient eddies, irrotational vorticity fluxes from anisotropy associated with systematic horizontal tilts and irrotational potential vorticity fluxes from either or both.

9) The only transient eddy fluxes that are predominantly irrotational are the lower tropospheric heat fluxes, which are systematically directed down the local horizontal gradient of mean temperature. We interpret these observational results as evidence

of the primacy of baroclinic instability as a driving mechanism for the transient eddies. The magnitudes of these fluxes are large enough to be of major importance in the local, time-averaged heat balance (Lau, 1979b). Despite the strong directional relationship between $\mathbf{F}(T)$ and $\nabla\bar{T}$ there is no observational evidence of a direct relationship between their absolute magnitudes. Apparently $|\mathbf{F}(T)|$ depends not only on $|\nabla\bar{T}|$, but also on other factors (e.g., some measure of the vertical stratification).

10) The other important pattern evident in the irrotational fluxes is the apparent relationship between the fluxes of relative vorticity and potential vorticity and the sea level pressure pattern, with the fluxes being directed toward low-pressure centers. A similar relationship is apparent in statistics derived from the GFDL general circulation model, as reported in Blackmon and Lau (1979). It is interesting to note that the fluxes associated with horizontal advection by the time-averaged flow at the jet stream level display a similar pattern and are about twice as large as the transient eddy fluxes. It appears as though both the eddies and the mean flow at the jet stream level may be subject to the influence of vorticity and potential vorticity sources and sinks in the lower troposphere, which affect higher levels through the action of thermally and frictionally induced ageostrophic flows. The dynamical mechanisms responsible for these relationships are in need of further elucidation.

Acknowledgments. We would like to thank James R. Holton, Yoshikazu Hayashi and Abraham H. Oort for helpful discussions, and the official reviewers for useful suggestions.

The work was supported by the Climate Dynamics Program, Climate Dynamics Research Section, Atmospheric Sciences Division, National Science Foundation under Grant 78-07369, and by the National Center for Atmospheric Research, which provided computer facilities and partial salary support for N.-C. Lau in the form of a graduate assistantship.

REFERENCES

Blackmon, M. L., and N-C. Lau, 1979: Regional characteristics of the Northern Hemisphere wintertime circulation: A comparison of a general circulation model with observations. Accepted for publication in *J. Atmos. Sci.*

Clapp, P. F., 1956: Some considerations involved in preparing long range forecasts by numerical methods. *J. Meteor.*, **13**, 341–350.

——, 1970: Parameterization of macroscale transient heat transport for use in a mean-motion model of the general circulation. *J. Appl. Meteor.*, **9**, 554–563.

Dopplick, T. G., 1974: Radiative heating in the atmosphere. *The General Circulation of the Tropical Atmosphere*, Vol. II, R. E. Newell *et al.*, Eds. The MIT Press, 1–25.

Hartmann, D. L., 1977: On potential vorticity and transport in the stratosphere. *J. Atmos. Sci.*, **34**, 968–977.

Holopainen, E. O., 1978: On the dynamic forcing of the long term mean flow by the large-scale Reynolds stresses in the atmosphere. *J. Atmos. Sci.*, **35**, 1596–1604.

Lau, N-C., 1978: On the three-dimensional structure of the observed transient eddy statistics of the Northern Hemisphere wintertime circulation. *J. Atmos. Sci.*, **35**, 1900–1923.

——, 1979a: The structure and energetics of transient disturbances in the Northern Hemisphere wintertime circulation. *J. Atmos. Sci.*, **36**, 982–995.

——, 1979b: The observed structure of tropospheric stationary waves and the local balances of vorticity and heat. *J. Atmos. Sci.*, **36**, 996–1016.

——, H. Tennekes and J. M. Wallace, 1978: Maintenance of the momentum flux by transient eddies in the upper troposphere. *J. Atmos. Sci.*, **35**, 139–147.

NCAR, 1978: NCAR software support library, Vol. 2. NCAR Tech. Note TN/IA-105.

Newell, R. E., J. W. Kidson, D. G. Vincent and G. J. Boer, 1972 and 1974: *The General Circulation of the Tropical Atmosphere*, Vols. I and II. The MIT Press, 258 and 370 pp.

Rosen, R. D., D. A. Salstein and J. P. Peixoto, 1979: Variability in the annual fields of large-scale atmospheric water vapor transport. *Mon. Wea. Rev.*, **107**, 26–37.

Saltzman, B., 1962: Empirical forcing functions for the large-scale mean disturbances in the atmosphere. *Geophys. Pura Appl.*, **52**, 173–188.

Shukla, J., and K. R. Saha, 1974: Computation of non-divergent streamfunction and irrotational velocity potential from the observed winds. *Mon. Wea. Rev.*, **102**, 419–425.

Starr, V. P., J. P. Peixoto and A. R. Crisi, 1965: Hemispheric water balance for the IGY. *Tellus*, **17**, 463–472.

Tucker, G. B., 1977: An observed relation between the macroscale local eddy flux of heat and the mean horizontal temperature gradient. *Quart. J. Roy. Meteor. Soc.*, **103**, 157–168.